Available online at www.sciencedirect.com
ScienceDirect
Trans. Nonferrous Met. Soc. China 33(2023) 2832−2842
Transactions of Nonferrous Metals Society of China
www.tnmsc.cn

Effect of CaO on zinc migration mechanism and kinetics during zinc ferrite reduction

Wei-an WANG, Guo-xing QIU, Jian-li WANG, Yun HE, Xiao-ming LI

School of Metallurgical Engineering, Xi'an University of Architecture and Technology, Xi'an 710055, China

Received 9 April 2022; accepted 5 July 2022

Abstract: Effects of CaO, reduction time and reduction temperature on the Zn migration mechanism and kinetic model were studied. Results show that CaO improves the volatilization rate of Zn by promoting the precipitation and enrichment of the intermediate product ZnO on the surface of the mixture of Fe and CaO. The reduction steps of $ZnFe_2O_4$ with CaO are $ZnFe_2O_4$→$Ca_2Fe_2O_5$→FeO→Fe. The volatilization model of the reduction of $ZnFe_2O_4$ was changed from a first-order chemical reaction model (without CaO) to a three-dimensional diffusion model (with CaO), and the apparent activation energy was reduced from 313.9 to 91.77 kJ/mol, providing favorable conditions for the efficient reduction and volatilization of zinc.

Key words: zinc-containing dust; zinc ferrite; reaction kinetics; migration mechanism; direct reduction; Zn recovery

1 Introduction

With the development of a circular economy, the recycling and utilization of the solid waste containing zinc are receiving increasing attention [1]. $ZnFe_2O_4$ is widely found as a spinel phase in zinc-containing solid waste such as copper metallurgy [2−4], zinc metallurgy [5,6], and steel production processes [7], and the specific chemical structure of $ZnFe_2O_4$ impacts the recovery of zinc-containing solid waste in both hydrometallurgy and pyrometallurgical process [8,9]. Meanwhile, the accumulation of these solid wastes is also an environmental hazard.

To efficiently treat zinc-containing solid waste containing $ZnFe_2O_4$ phase and recover zinc resources, some researchers have done a lot of work. YU et al [10] and PENG et al [11] transformed $ZnFe_2O_4$ in zinc leaching residues into low-valent iron oxides and ZnO by the reduction of roasting in the CO atmosphere to improve the zinc recovery. GRUDINSKY et al [12] suggested that the zinc recovery was improved by mixing zinc plant residue with iron sulfates for sulfide roasting to convert the $ZnFe_2O_4$ to iron oxides and $ZnSO_4$. HU et al [13] reported that zinc leaching residues and jarosite residues ($KFe_3(SO_4)_2(OH)_6$) were mixed and roasted to convert $ZnFe_2O_4$ phase to $ZnSO_4$ for zinc recycling. MIKI et al [14] proposed roasting treatment with CaO in the electric furnace dust to convert the $ZnFe_2O_4$ phase into an easily leachable ZnO phase, resulting in a significant improvement in zinc recovery. CHAIRAKSA et al [15] added CaO into EAF dust. $ZnFe_2O_4$ was converted to $CaFe_2O_4$ and easily reduced ZnO phases during the reduction process, which improved the volatilization of zinc. In addition, GAN et al [16] showed that the Zn-containing phase could be changed by CaO during the sintering process to improve the removal of zinc from the sintered ore. XIA et al [17] found that CaO in the dust sludge could promote the volatilization of the Zn-containing phase during the mixed roasting of the gravity dust

Corresponding author: Xiao-ming LI, Tel: +86-18702982898, Fax: +86-29-82202923, E-mail: xmli@xauat.edu.cn;
Guo-xing QIU, Tel: +86-18609826879, E-mail: guoxingqiu2008@126.com
DOI: 10.1016/S1003-6326(23)66301-0

and converter sludge. ITOH et al [18] suggested magnetizing roasting of electric furnace ash with CaO to convert $ZnFe_2O_4$ into ZnO and Fe_3O_4, then magnetic separation of zinc and iron. Moreover, LV et al [19] found that the rate of zinc volatilization for Fe_3O_4−ZnO−CaO mixtures was higher than that for Fe_3O_4−ZnO mixtures in the same CO atmosphere.

Transformation of the $ZnFe_2O_4$ phase into the easily recoverable ZnO phase is an effective method to improve the recovery of Zn from solid waste. However, the effect of CaO on the mechanism of $ZnFe_2O_4$ reduction is currently studied by indirect reasoning and needs further thorough investigation. In this work, the effect of CaO on the migration behavior of zinc elements in $ZnFe_2O_4$ carbon thermal reduction was investigated, and the effect of CaO on the kinetic model of $ZnFe_2O_4$ carbon thermal reduction zinc volatilization was investigated, which clarified the mechanism of CaO promoting the volatilization of zinc in $ZnFe_2O_4$. All those are important for improving the recycling of $ZnFe_2O_4$-containing solid waste and increasing the recovery rate of zinc.

2 Experimental

2.1 Materials

Zinc ferrite was prepared with zinc oxide and hematite as raw materials according to the previous published methods [20]. The zinc oxide and hematite mixture were roasted at 1000 °C in an air flow for 4 h and washed in HCl solution. The XRD pattern of $ZnFe_2O_4$ is shown in Fig. 1. There are no other diffraction peaks except $ZnFe_2O_4$, which is also reported by other literature with the same preparation method of $ZnFe_2O_4$ [21,22]. The reducing agent was pure graphite and CaO was reagent pure during the experiment.

2.2 Experimental methods and equipment

The high-temperature reduction experiment was carried out in a horizontal tube furnace. First, zinc ferrite, CaO, and graphite powder were mechanically mixed according to Zn/Ca molar ratio 1:1 and C/O molar ratio 1:1 (15.69 wt.% CaO; 16.81 wt.% C). The mixture was pressed into cylindrical samples with a diameter of d15 mm × 10 mm, and the mass of each sample was (4±0.1) g. Argon gas was used to purge the furnace before the start of the experiment. Next, the temperature was raised to the experimental temperatures (950, 1000, 1050, and 1100 °C), and the porcelain boat filled with the sample (4×4 g) was pushed into the high-temperature zone for reaction. Ar was used as the protective gas at a flow rate of 1.0 L/min.

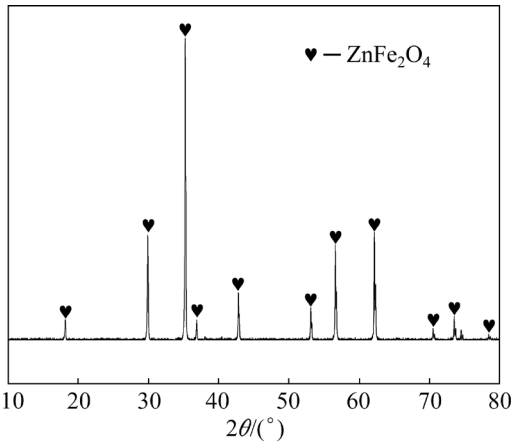

Fig. 1 XRD pattern of zinc ferrite

After the experiment, the product was quickly taken out, cooled by liquid nitrogen, and ground for subsequent analysis and detection. The volatilization rate of zinc was calculated according to Eq. (1):

$$Q=\frac{m_0w_0-m_1w_1}{m_0w_0}\times100\% \quad (1)$$

where Q is the volatilization rate (%) of Zn, m_0 is the mass of the example before reaction (g), w_0 is the mass fraction (%) of Zn in the example before reaction, m_1 is the mass (g) of the product after reaction, and w_1 is the mass fraction (%) of Zn in the product after the reaction.

2.3 Zinc volatility kinetics

The effect of CaO on the reduction of $ZnFe_2O_4$ was carried out by the isothermal kinetic method. The volatilization rate of zinc (Q) can be expressed by the differential of the volatilization rate of zinc (α) and reduction time (t):

$$Q=\mathrm{d}\alpha/\mathrm{d}t=K(T)\cdot f(\alpha) \quad (2)$$

$$G(\alpha)=\int_0^t K(T)\mathrm{d}t=K(T)t \quad (3)$$

where Eq. (3) is the integral form of Eq. (2); $K(T)$ is the apparent reaction rate which is determined by the reduction temperature T; $f(\alpha)$ is the mechanical function; $G(\alpha)$ is the integral form of $f(\alpha)$.

The isothermal kinetic models used in this study are listed in Table 1, including the diffusion model, Avrami–Erofeev equation, chemical reaction model, and shrinking core model. According to the results of different temperatures and time, the model function $G(\alpha)$ was fitted linearly. The activation energy of the reaction process is calculated by fitting $\ln K(T)$ to $-1/(RT)$ after the mechanism function $K(T)$ is obtained [23−25].

$$K(T)=A\exp[-E_a/(RT)] \quad (4)$$

$$\ln K(T)=-E_a/(RT)+\ln A \quad (5)$$

where E_a is the apparent activation energy (kJ/mol); A is the pre-exponential factor (min^{-1}); R is the molar gas constant; T is the reduction temperature (K).

2.4 Material characterization

The zinc content in samples was determined by using X-ray Fluorescence(XRF) spectrometer (ZSXPrimus Japan). The phase composition in the samples was investigated through the X-ray diffraction (XRD, Bruker D8 Advance Germany). The scanning rate was 3 (°)/min, and the scanning range was 10°−80°. The microstructure of the specimen and the reaction product were observed on a scanning electron microscope (SEM; GeminiSEM500, Germany) with an energy dispersive spectrometer (EDS; UltimMax100, Oxford Instruments, UK).

3 Results and discussion

3.1 Effect of CaO on volatility of zinc

Figure 2 shows the effect of CaO on the volatility of zinc at different reduction temperatures and reduction time. As shown in Fig. 2(a), when the reduction temperature is lower than 1050 °C, the volatilization rate of zinc without CaO increases slowly. However, the volatilization rate of zinc increases rapidly with time at 1100 °C. When the temperature is higher than 1100 °C, the gasification reaction of carbon (graphite) occurs rapidly [26], resulting in increased CO content in the atmosphere, and the volatilization rate of zinc is controlled from

Table 1 Common algebraic expressions of $f(\alpha)$ and $G(\alpha)$ for kinetic models used

Code	Mechanism	Kinetic model	Integral $G(\alpha)$	Differential $f(\alpha)$
D_1	Diffusion	One-dimensional diffusion	α^2	$1/(2\alpha)$
D_2		Two-dimensional diffusion, cylindrical symmetry	$\alpha+(1-\alpha)\ln(1-\alpha)$	$[-\ln(1-\alpha)]^{-1}$
D_3		Three-dimensional diffusion, spherical symmetry	$[1-(1-\alpha)^{1/3}]^2$	$3/2(1-\alpha)^{2/3}[1-(1-\alpha)^{1/3}]^{-1}$
D_4		Three-dimensional diffusion, cylindrical symmetry	$1-(2/3)\alpha-(1-\alpha)^{2/3}$	$(3/2)[(1-\alpha)^{-1/3}-1]^{-1}$
D_5		Three-dimensional diffusion	$[(1+\alpha)^{1/3}-1]^2$	$(3/2)(1+\alpha)^{2/3}[(1+\alpha)^{1/3}-1]^{-1}$
D_6		Three-dimensional diffusion	$[(1-\alpha)^{-1/3}-1]^2$	$(3/2)(1-\alpha)^{4/3}[(1-\alpha)^{-1/3}-1]^{-1}$
A_1	Random nucleation and nuclei growth	Avrami–Erofeev, n=1/3	$[-\ln(1-\alpha)]^{1/3}$	$3(1-\alpha)[-\ln(1-\alpha)]^{2/3}$
A_2		Avrami–Erofeev, n=1/2	$[-\ln(1-\alpha)]^{1/2}$	$2(1-\alpha)[-\ln(1-\alpha)]^{1/2}$
A_3		Avrami–Erofeev, n=3/2	$[-\ln(1-\alpha)]^{3/2}$	$(2/3)(1-\alpha)[-\ln(1-\alpha)]^{-1/2}$
A_4		Avrami–Erofeev, n=2	$[-\ln(1-\alpha)]^2$	$(1/2)(1-\alpha)[-\ln(1-\alpha)]^{-1}$
A_5		Avrami–Erofeev, n=3	$[-\ln(1-\alpha)]^3$	$(1/3)(1-\alpha)[-\ln(1-\alpha)]^{-2}$
C_1	Chemical reaction	First-order	$-\ln(1-\alpha)$	$1-\alpha$
C_2		Second-order	$(1-\alpha)^{-1}-1$	$(1-\alpha)^2$
C_3		Third-order	$[(1-\alpha)^{-2}-1]^2$	$(1-\alpha)^3$
R_1	Shrinking core	Phase boundary reaction, cylindrical symmetry	$1-(1-\alpha)^{1/2}$	$2(1-\alpha)^{1/2}$
R_2		Phase boundary reaction, spherical symmetry	$1-(1-\alpha)^{1/3}$	$3(1-\alpha)^{2/3}$

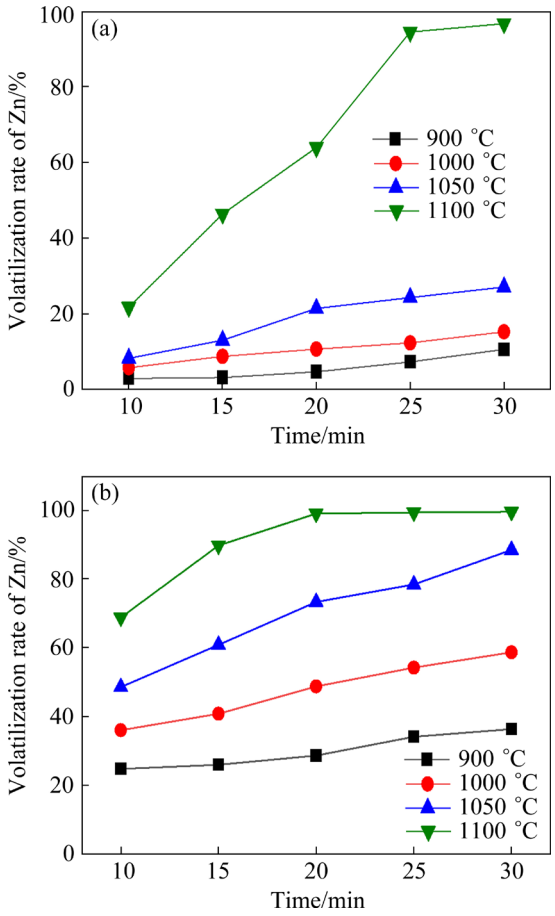

Fig. 2 Effect of CaO on volatility of zinc at different reduction temperatures and time: (a) Without CaO; (b) With CaO

solid−solid reaction to gas−solid reaction. Figure 2(b) contains the volatilization rate of zinc with CaO at different temperatures and time. The volatilization rate of zinc increases slowly with time at the same temperature. The reduction temperature has a significant influence on the volatilization rate of zinc.

When the temperature was below 1050 °C without CaO, the highest volatilization rate of zinc was 27.16%. However, the lowest volatilization rate with CaO was 36.41%, when the temperature was 950 °C for 10 min. When the temperature was 1100 °C for 30 min, the volatility of zinc reached 96.61% without CaO. The volatility of zinc reached 99% with CaO, when the sample was reduced for 20 min at the same temperature. CaO could decrease the reduction temperature and reduction time. The gasification temperature of the carbon is decreased by CaO, which increases the concentration of CO in the reducing atmosphere and decreases the temperature of Zn sublimation [9,15].

3.2 Kinetics of zinc volatilization

The fitting results of different mechanism functions $G(\alpha)$ with time are calculated according to the experimental results of Fig. 2, which are shown in Table 2. According to the fit R^2 at different temperatures in Table 2, the maximum value of R^2 is the kinetic mechanism function of the reaction process. The reduction of $ZnFe_2O_4$ without CaO is controlled by the first-order chemical reaction model. When CaO is added, the reduction of $ZnFe_2O_4$ is controlled by the three-dimensional diffusion model.

The calculation of apparent activation energy is shown in Section 2.3. The results of fitting ln K to $1/T$ by Eq. (5) are shown in Fig. 3, and the apparent activation energy is shown in Table 3. When there is no CaO, the apparent activation energy required for the reduction of $ZnFe_2O_4$ is 313.90 kJ/mol, which is consistent with the magnitude of carbon thermal reduction activation energy reported in the literature for pure $ZnFe_2O_4$ [27]. The apparent activation energy required for the reduction of $ZnFe_2O_4$ is reduced to 91.77 kJ/mol with CaO. The reason is that CaO converts $ZnFe_2O_4$ into $CaFe_2O_4$. LI et al [28] found that the activation energy of $CaFe_2O_4$ is much lower than $ZnFe_2O_4$. Zinc is more easily recovered.

3.3 Evolution of zinc-containing phases

3.3.1 Effect of reduction time

XRD patterns of the reduction products after different time at 1050 °C are shown in Fig. 4. When zinc ferrite was reduced with CaO for 10 min, $Ca_2Fe_2O_5$ and ZnO diffraction peaks appeared. Meanwhile, the $ZnFe_2O_4$ diffraction peak disappeared, which indicated that CaO could replace the zinc in $ZnFe_2O_4$. The diffraction peak of Fe appears at 10 min, the reason is that CaO promotes the gasification reaction of carbon and increases the partial pressure of CO in the atmosphere [29], which not only promotes the reduction of the iron oxide but also decreases the conversion temperature of ZnO to Zn(g) [30]. With the increase of reduction time, the diffraction peaks of $Ca_2Fe_2O_5$ and FeO decrease, while the diffraction peak of Fe is increased. The intensity of the Fe diffraction peak is maximum and the CaO diffraction peak reappears after 30 min, as well as the diffraction peak of slight FeO. Compared with the reaction without CaO for 30 min, the diffraction

Table 2 Data-fitting results determined by model-fitting method under different condition

Condition	T/°C	R^2							
		D_1	D_2	D_3	D_4	D_5	D_6	A_1	A_2
Without CaO	950	0.90921	0.90752	0.90579	0.90695	0.91219	0.90232	0.97451	0.96983
	1000	0.98649	0.98533	0.98408	0.98492	0.98824	0.98141	0.98732	0.99032
	1050	0.98863	0.98922	0.98969	0.98940	0.98764	0.99019	0.96771	0.97211
	1000	0.97138	0.95764	0.93787	0.95077	0.97682	0.90448	0.98221	0.97806
With CaO	950	0.97098	0.96979	0.96848	0.96935	0.97734	0.96574	0.97656	0.97656
	1000	0.99648	0.99594	0.99459	0.99557	0.99683	0.98954	0.99673	0.99634
	1050	0.99324	0.99175	0.97460	0.98734	0.99424	0.91019	0.99123	0.99315
	1100	0.86105	0.89220	0.93501	0.90997	0.93524	0.90736	0.64126	0.93121
Condition	T/°C	R^2							
		A_3	A_4	A_5	C_1	C_2	C_3	R_1	R_2
Without CaO	950	0.92922	0.90406	0.85385	0.97755	0.95681	0.95248	0.95312	0.95269
	1000	0.99166	0.98278	0.95275	0.99183	0.98384	0.98449	0.98446	0.98448
	1050	0.98803	0.99001	0.98488	0.99450	0.97421	0.98135	0.98043	0.98105
	1000	0.93670	0.92115	0.90245	0.98224	0.93334	0.96838	0.97642	0.97145
With CaO	950	0.97095	0.96714	0.95875	0.97443	0.97252	0.97299	0.97254	0.97517
	1000	0.99557	0.99248	0.98160	0.99681	0.99128	0.99644	0.99661	0.99679
	1050	0.96843	0.94686	0.89685	0.98457	0.95550	0.99139	0.99412	0.99284
	1100	0.92506	0.91031	0.90825	0.92787	0.90144	0.92901	0.90527	0.82163

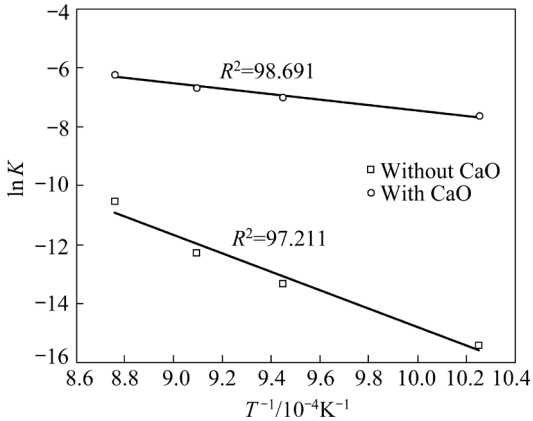

Fig. 3 Arrhenius plots of ln K vs T^{-1} of kinetic models

Table 3 Kinetic parameters of zinc volatilization under different conditions

Condition	Mechanism function	E_a/(kJ·mol^{-1})
Without CaO	$-\ln(1-\alpha)$	313.90
With CaO	$[(1+\alpha)^{1/3}-1]^2$	91.77

peak of ZnO disappeared, and the volatilization rate of zinc also increased to 88.47%.

CaO converts $ZnFe_2O_4$ into ZnO and $CaFe_2O_5$, which not only promotes the reduction of ZnO and increases the volatility of zinc, but also promotes the reduction of iron oxides to metallic iron.

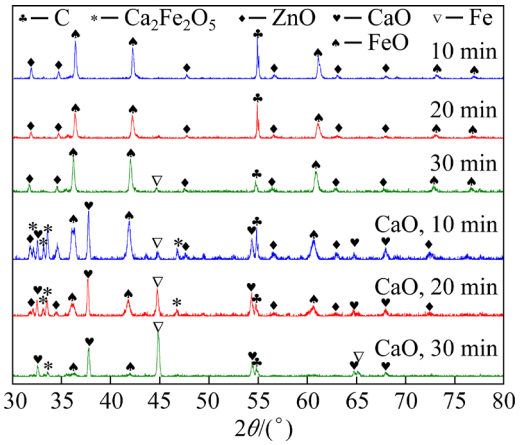

Fig. 4 XRD patterns of reduction products after different reduction time at 1050 °C

3.3.2 Effect of reduction temperature

XRD patterns of the reduction products are shown in Fig. 5, which were prepared at different temperatures for 30 min. The phase analysis results of the sample without CaO are shown in Fig. 5(a). The results showed that $ZnFe_2O_4$ was reduced to ZnO and Fe_3O_4 by carbon at 950 °C. The diffraction peak intensity of ZnO was the strongest and the volatility of zinc was 10.68%. With the increase of temperature to 1000 °C, the diffraction peaks of

Fe_3O_4 disappeared while the diffraction peaks of FeO appeared. The ZnO diffraction peak intensity also decreased with the increase of the volatility of zinc. The diffraction peak intensity of FeO decreased further in the reduced product at 1050 °C, while Fe-diffraction peaks began to appear faintly. When the temperature was increased to 1100 °C, there were only Fe diffraction peak and residual carbon diffraction peak remained in the reduction products. ZnO was not found in the product, and the volatility of Zn reached 96.61%. In summary, the reduction of $ZnFe_2O_4$ without CaO follows the stepwise reduction of iron oxides $ZnFe_2O_4$→Fe_3O_4→FeO→Fe, where the reduction of zinc follows $ZnFe_2O_4$→ZnO→Zn(g).

The phase analysis results of samples with CaO are shown in Fig. 5(b). $ZnFe_2O_4$ was reduced to $CaFe_2O_4$, ZnO, and low valent iron oxide (FeO) at 950 °C for 30 min. The diffraction peak intensity of $Ca_2Fe_2O_5$ decreases with the temperature increasing to 1000 °C. The diffraction peak intensity

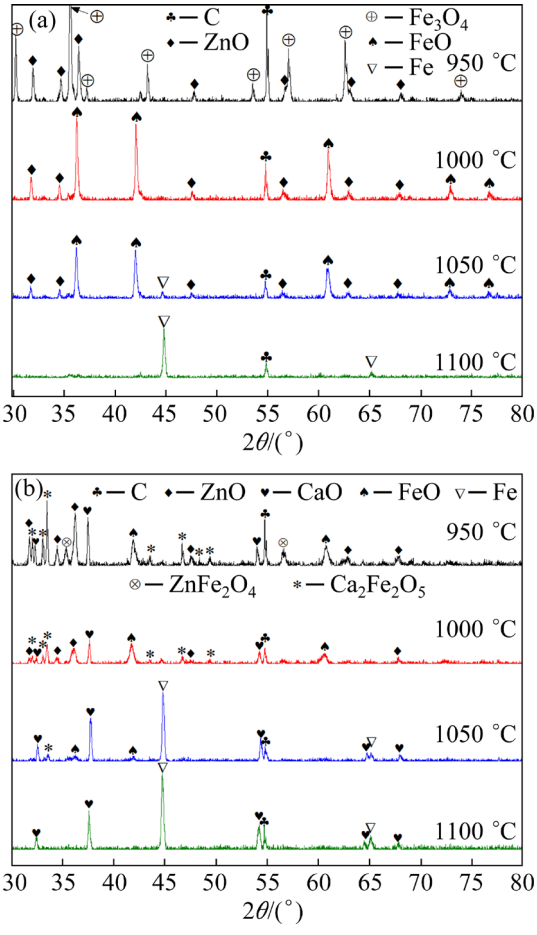

Fig. 5 XRD patterns of reduction products at different reduction temperatures: (a) $ZnFe_2O_4$ without CaO for 30 min; (b) $ZnFe_2O_4$ with CaO for 30 min

of ZnO also decreases with the rising volatility of zinc. When the temperature was increased to 1050 °C, the volatility of zinc was 88.47% and the diffraction peak of ZnO almost disappeared. The diffraction peak intensity of Fe increased rapidly due to the reduction of $CaFe_2O_4$. Meanwhile, the diffraction peaks of FeO and CaO appear. The diffraction peak of $Ca_2Fe_2O_5$ disappeared completely at 1100 °C, and diffraction peaks of CaO, Fe, and residual carbon were remained.

After CaO was added, the reduction of iron-containing phases did not follow the stepwise reduction of iron oxidation ($ZnFe_2O_4$→Fe_3O_4→FeO→Fe), but followed $ZnFe_2O_4$→$Ca_2Fe_2O_5$→FeO→Fe, which is consistent with the results in the literature [31]. CaO not only increases the volatility of zinc, but also catalyzes the gasification reaction of carbon, and increases the concentration of CO to promote the reduction of iron oxide.

3.4 Zinc migration and morphological evolution

The SEM images of raw materials is shown in Fig. 6. The dark part is graphite, and the white granular is $ZnFe_2O_4$ powder (Fig. 6(a)). The dark part is graphite, and the white particle is a mixture of $ZnFe_2O_4$ and CaO powder (Fig. 6(b)). Zinc elements in the two samples initial state were evenly distributed without aggregation.

The SEM images of $ZnFe_2O_4$ without CaO are shown in Fig. 7. Figure 7(a) shows the microscopic morphology of the sample after 10 min reduction without CaO. The sample appeared to be sintered, in which the distribution of zinc was as uniform as that in the raw material. The sintering phenomenon inhibits the formation of pores and hinders the gasification reaction of carbon at high temperatures, thus inhibiting the reaction of ZnO with CO. The volatilization rate of zinc is mainly determined by the solid−solid reaction rate of ZnO with carbon, the volatility of zinc was 8.33%. The sample surface was dense and flat after 20 min reduction at 1050 °C (Fig. 7(b)), and only a few pores were produced at the junction of carbon and $ZnFe_2O_4$, which were mainly made by the gases generated by the reaction. Zn, Fe and C elements were uniformly distributed, and the volatility of zinc increased by 4.78% compared with the sample at 10 min.

The surface of sample without CaO becomes more densely and flatly with the increase of

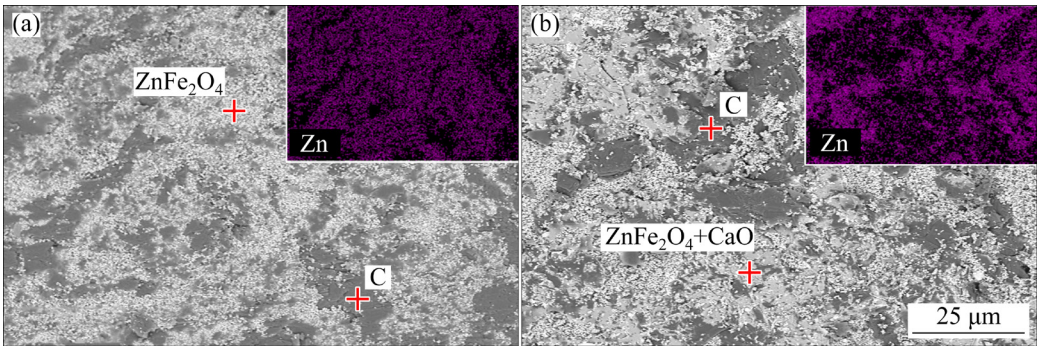

Fig. 6 SEM images of raw samples: (a) Without CaO; (b) With CaO

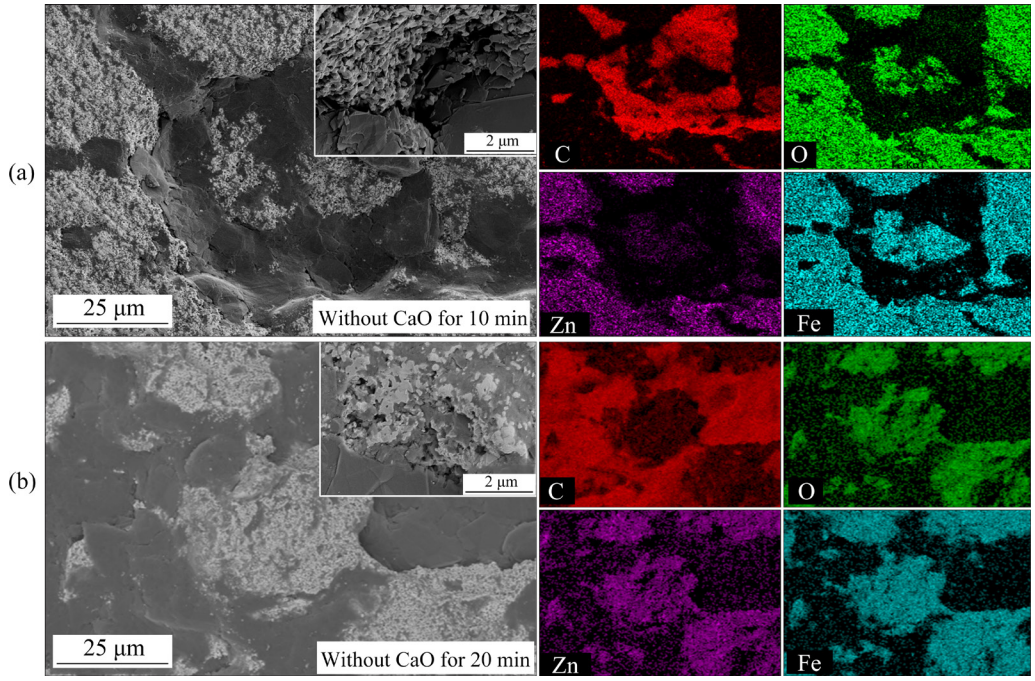

Fig. 7 SEM images of $ZnFe_2O_4$ reduction at 1050 °C

reduction time, which prevents the generation of CO_2 from reaction of carbon and CO, causing the gas-solid reduction not to be carried out. The volatilization rate of zinc is determined by the solid−solid reaction of ZnO with C, resulting in a lower volatilization rate of zinc, which corresponds to the first-order chemical reaction model obtained by kinetic calculations in Section 3.2.

Figure 8 shows that the surface of sample with CaO is uneven with abundant pores. Meanwhile, there was an obvious enrichment in the distribution of zinc elements compared with sample without CaO. Figure 8(b) shows that the reduction of the sample by adding CaO for 10 min results in a layered structure. The Zn/O molar ratio is close to 1 in Point 2, and the surface layer is inferred to be ZnO. The Ca/O molar ratio of the inner layer structure is close to 1. Therefore, the material is a mixture with CaO and metal Fe, which is consistent with the results in Fig. 4 (CaO-1050 °C-10 min). The reason is that Ca atoms replace Zn atoms and CaO promotes the enrichment of Zn elements on the surface of CaO and Fe mixture, which provides favorable conditions for the volatilization of zinc.

The morphology evolution of $ZnFe_2O_4$ with CaO for 20 min is shown in Fig. 9. Compared with the reduction at 1050 °C for 10 min, the zinc volatilization rate increased by 24.76%, and the zinc element was distributed in sporadic clusters in Fig. 9(a). The reason was that ZnO enriched on the surface of the mixture of CaO and Fe in the early stage was reduced. Figure 9(b) shows the precipitation

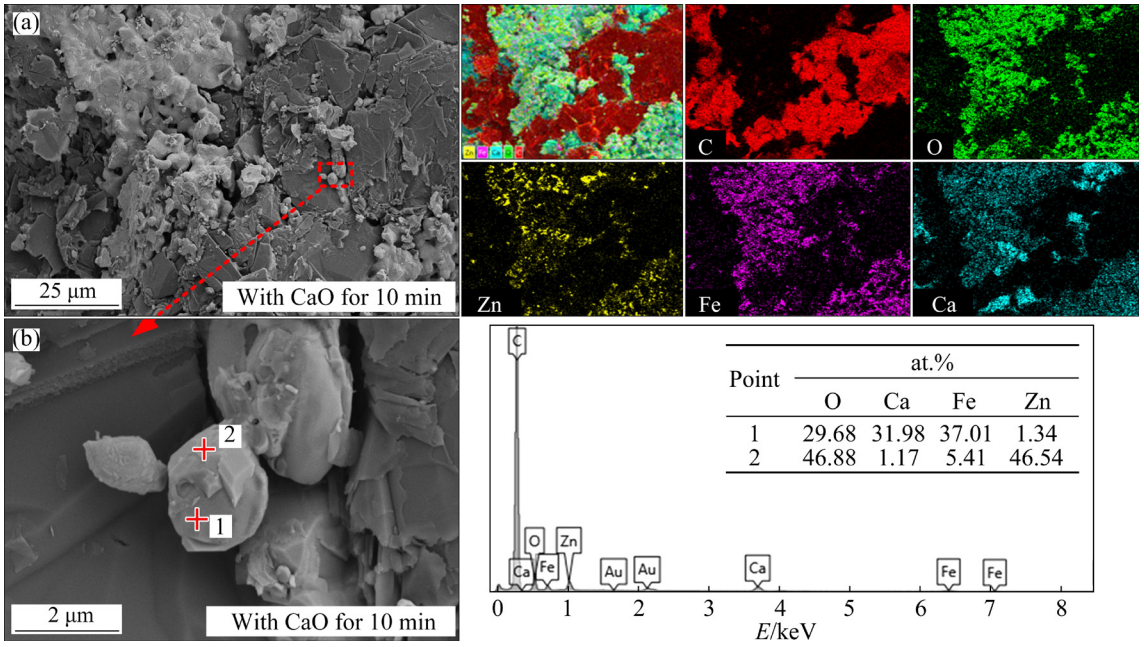

Fig. 8 SEM images of $ZnFe_2O_4$ with CaO for 10 min: (a) Macro morphology; (b) Enlarged view of (a)

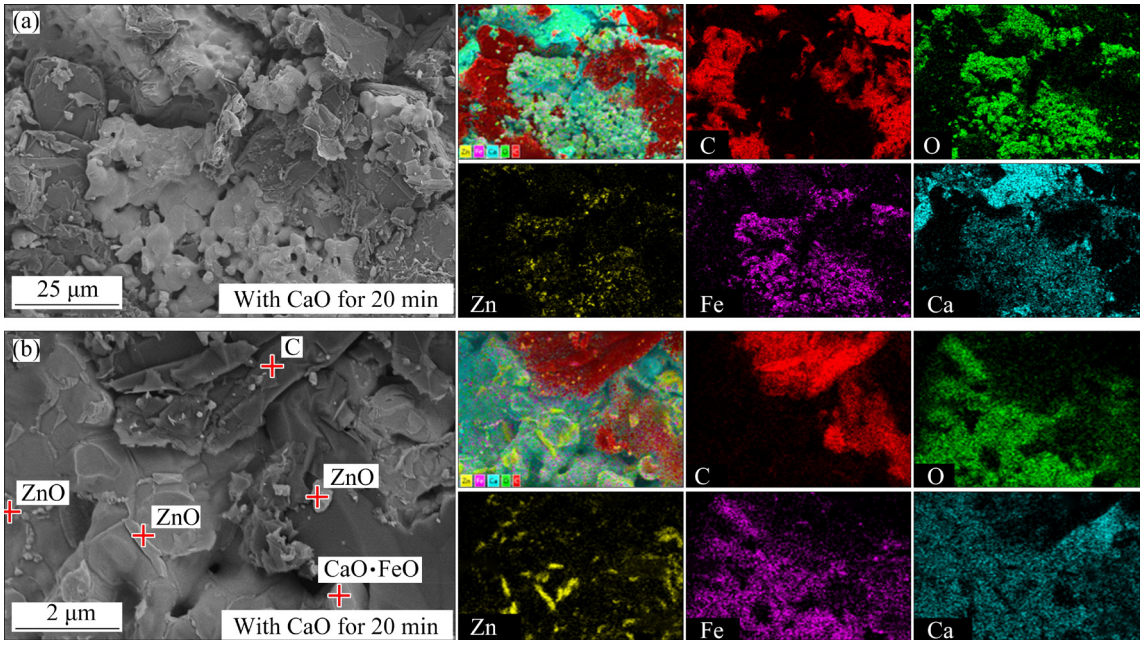

Fig. 9 SEM images of $ZnFe_2O_4$ with CaO for 20 min: (a) Macro morphology; (b) Enlarged view of (a)

of striped and dotted ZnO clusters on the surface of the Fe and CaO mixture (the light gray area), further demonstrating that the addition of CaO can displace the Zn elements in $ZnFe_2O_4$ and promote the enrichment and volatilization of zinc.

3.5 Mechanism of zinc migration

Mechanism diagram of $ZnFe_2O_4$ reduction enhanced by CaO is shown in Fig. 10. The reduction process of $ZnFe_2O_4$ without CaO is shown in Fig. 10(a). $ZnFe_2O_4$ decomposed into ZnO and low-valent iron oxides (Fe_mO_n) at 1050 °C for 10 min, and ZnO was easily reduced [32]. However, the volatilization of zinc was only 8.33%. The reason is that poor kinetic conditions limited the reduction of ZnO. Kinetic calculations (Section 3.2) show that the volatilization of zinc of sample without CaO is controlled by the first-order chemical reaction model. Moreover, the reduction products started to melt, inhibiting the formation of

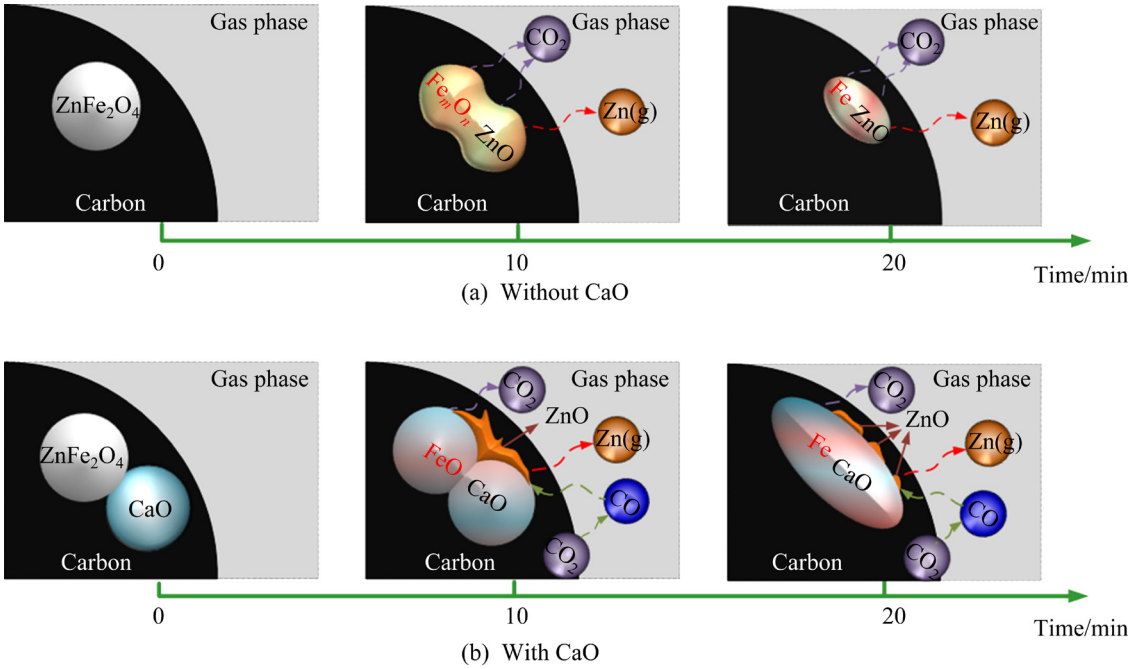

Fig. 10 Mechanism diagram of $ZnFe_2O_4$ reduction enhanced by CaO

pores and hindering the gasification reaction of CO_2 with carbon, thereby inhibiting the ZnO reaction with CO. The reduction volatilization rate of ZnO depended on the solid−solid reaction rate of ZnO with carbon, so the volatilization rate of zinc is lower. After the sample was reduced for 20 min, the reduction product sintering was further aggravated and the medium product ZnO could not contact the reducing agent, which caused a lot of medium product ZnO not to be reduced.

The reduction of $ZnFe_2O_4$ with CaO is shown in Fig. 10(b), $ZnFe_2O_4$, CaO and C mixed well, and zinc elements were uniformly distributed. After the sample was reduced at 1050 °C for 10 min, CaO reacted with $ZnFe_2O_4$ to form $CaFe_2O_4$ and ZnO. In addition, the reduction of iron oxides to form monomeric Fe was also promoted (Fig. 4), which is because CaO reduced the apparent activation energy of $ZnFe_2O_4$ reduction from 313.9 to 91.77 kJ/mol. CaO promoted the enrichment of the intermediate product ZnO on the surface of the Fe and CaO mixture (Fig. 8), which was beneficial to the volatilization of zinc. ZnO reduction is no longer the limiting link. Kinetic calculations show that the reduction of $ZnFe_2O_4$ with CaO is controlled by a three-dimensional diffusion model. With the increase in reduction temperature, the saturated vapor pressure of zinc increases [30], which is conducive to the diffusion and volatilization of the reduced monomeric zinc, and the volatilization rate of zinc increases from 8.33% to 48.60% under the same conditions. A large amount of Fe and CaO mixture was generated within 20 min, and ZnO was still aggregated on the surface of the mixture. Moreover, CaO can further catalyze the gasification reaction of CO_2 with carbon [33,34], which increases the CO concentration in the reaction system and promotes the reaction of surface aggregated ZnO with CO to improve the volatility of zinc.

4 Conclusions

(1) When CaO is not added, the carbon thermal reduction of $ZnFe_2O_4$ is controlled by the first-order chemical reaction model with the mechanical function of $f(\alpha)=-\ln(1-\alpha)$, and the apparent activation energy is 313.90 kJ/mol. When CaO is added, the carbon thermal reduction of $ZnFe_2O_4$ is controlled by the three-dimensional diffusion model with the mechanical function of $f(\alpha)=[(1+\alpha)^{1/3}-1]^2$, and the apparent activation energy was reduced to 91.77 kJ/mol.

(2) The reduction of $ZnFe_2O_4$ without CaO follows the stepwise reduction: $ZnFe_2O_4 \rightarrow Fe_3O_4 \rightarrow FeO \rightarrow Fe$. The reduction of $ZnFe_2O_4$ with CaO follows $ZnFe_2O_4 \rightarrow Ca_2Fe_2O_5 \rightarrow FeO \rightarrow Fe$.

(3) The volatilization mechanism of Zn in

$ZnFe_2O_4$ is affected by CaO. Without CaO, the Zn elements in the sample are always distributed diffusely and uniformly with time increasing, while volatilization of Zn is hindered by the melting of the sample. The kinetic conditions for the reduction of $ZnFe_2O_4$ are improved by CaO. CaO promoted the enrichment of the intermediate product ZnO on the surface of the Fe and CaO mixture. Meanwhile, it is helpful for the gas−solid reduction and solid−solid reduction reactions of ZnO, thus increasing the volatility of zinc.

Acknowledgments

This work is supported by the Natural Science Basic Research Plan in Shaanxi Province, China (No.2019JLM-35), and the Key Laboratory of Ecological Metallurgy of Multimetallic Mineral (Northeastern University) of the Ministry of Education, China.

References

[1] ZHU Xiao-lin, XU Cun-ying, TANG Jie, HUA Yi-xin, ZHANG Qi-bo, LIU Hai, WANG Xiang, HUANG Meng-ting. Selective recovery of zinc from zinc oxide dust using choline chloride based deep eutectic solvents [J]. Transactions of Nonferrous Metals Society of China, 2019, 29(10): 2222−2228.

[2] ORAC D, LAUBERTOVA M, PIROSKOVA J, KLEIN D, BURES R, KLIMKO J. Characterization of dusts from secondary copper production [J]. Journal of Mining and Metallurgy Section B: Metallurgy, 2020, 56(2): 221−228.

[3] TIAN Hong-yu, GUO Zheng-qi, PAN Jian, ZHU De-qing, YANG Cong-cong, XUE Yu-xiao, LI Si-wei, WANG Ding-zheng. Comprehensive review on metallurgical recycling and cleaning of copper slag [J]. Resources Conservation and Recycling, 2021, 168: 105366.

[4] ZHANG Bei-kai, GUO Xue-yi, WANG Qin-meng, TIAN Qing-hua. Thermodynamic analysis and process optimization of zinc and lead recovery from copper smelting slag with chlorination roasting [J]. Transactions of Nonferrous Metals Society of China, 2021, 31(12): 3905−3917.

[5] LI Yan-chun, LIU Hui, PENG Bing, MIN Xiaobo, HU Min, PENG Ning, YUANG Ying-zhen, LEI Jie. Study on separating of zinc and iron from zinc leaching residues by roasting with ammonium sulphate[J]. Hydrometallurgy, 2015, 158: 42−48.

[6] HU Hui-ping, DENG Qiu-feng, LI Chao, XIE Yue, DONG Ze-qin, ZHANG Wei. The recovery of Zn and Pb and the manufacture of lightweight bricks from zinc smelting slag and clay [J]. Journal of Hazardous Materials, 2014, 271: 220−227.

[7] KAYA M, HUSSAINI S, KURSUNOGLU S. Critical review on secondary zinc resources and their recycling technologies [J]. Hydrometallurgy, 2020, 195: 105362.

[8] LANGOVÁ Š, LEŠKO J, MATÝSEK D. Selective leaching of zinc from zinc ferrite with hydrochloric acid [J]. Hydrometallurgy, 2009, 95(3/4): 179−182.

[9] CHAIRAKSA-FUJIMOTO R, MARUYAMA K, MIKI T, NAGASAKA T. The selective alkaline leaching of zinc oxide from Electric Arc Furnace dust pre-treated with calcium oxide [J]. Hydrometallurgy, 2016, 159: 120−125.

[10] YU Gang, PENG Ning, ZHOU Lan, LIANG Yan-jie, ZHOU Xiao-yuan, PENG Bing, CHAI Li-yuan, YANG Zhi-hui. Selective reduction process of zinc ferrite and its application in treatment of zinc leaching residues [J]. Transactions of Nonferrous Metals Society of China, 2015, 25(8): 2744−2752.

[11] PENG Bing, PENG Ning, MIN Xiao-bo, LIU Hui, LI Yan-chun, CHEN Dong, XUE Ke. Separation of zinc from high iron-bearing zinc calcines by reductive roasting and leaching [J]. JOM, 2015, 67(9): 1988−1996.

[12] GRUDINSKY P, PANKRATOV D, KOVALEV D, GRIGOREVA D, DYUBANOV V. Comprehensive study on the mechanism of sulfating roasting of zinc plant residue with iron sulfates [J]. Materials, 2021, 14(17): 5020.

[13] HU Ming, PENG Bing, CHAI Li-yuan, LI Yan-chun, PENG Ning, YUAN Ying-zhen, CHEN Dong High-zinc recovery from residues by sulfate roasting and water leaching [J]. JOM, 2015, 67(9): 2005−2012.

[14] MIKI T, CHAIRAKSA-FUJIMOTO R, MARUYAMA K, NAGASAKA T. Hydrometallurgical extraction of zinc from CaO treated EAF dust in ammonium chloride solution [J]. Journal of Hazardous Materials, 2016, 302: 90−96.

[15] CHAIRAKSA-FUJIMOTO R, INOUE Y, UMEDA N, ITOH S, NAGASAKA T. New pyrometallurgical process of EAF dust treatment with CaO addition [J]. International Journal of Minerals, Metallurgy, and Materials, 2015, 22(8): 788−797.

[16] GAN Min, JI Zhi-yun, FAN Xiao-hui, CHEN Xu-ling, ZHOU Yang, WANG Guo-jing, TIAN Ye, JIANG Tao. Clean recycle and utilization of hazardous iron-bearing waste in iron ore sintering process [J]. Journal of Hazardous Materials, 2018, 353: 381−392.

[17] XIA Lei-ge, MAO Rui, ZHANG Jian-liang, XU Xiang-nan, WEI Meng-fang, YANG Fei-hua. Reduction process and zinc removal from composite briquettes composed of dust and sludge from a steel enterprise [J]. International Journal of Minerals, Metallurgy, and Materials, 2015, 22: 122−131.

[18] ITOH S, TSUBONE A, MATSUBAE-YOKOYAMA K, NAKAJIMA K, NAGASAKA T. New EAF dust treatment process with the aid of strong magnetic field [J]. ISIJ International, 2008, 48(10): 1339−1344.

[19] LV Wei, GAN Min, FAN Xiao-hui, JI Zhi-yun, CHEN Xu-ling. Mechanism of calcium oxide promoting the separation of zinc and iron in metallurgical dust under reducing atmosphere [J]. Journal of Materials Research and Technology, 2019, 8(6): 5745−5752.

[20] ZHANG Lin-ye, MO Jia-mei, LI Xuan-hai, PAN Liu-ping, LIANG Xin-yuan, WEI Guang-tao. A kinetic study of indium leaching from indium-bearing zinc ferrite under microwave heating [J]. Metallurgical and Materials Transactions B, 2013, 44(6): 1329−1336.

[21] WANG Gong-liang, MIN Xiao-bo, PENG Ning, WANG Zhong-bing. The isothermal kinetics of zinc ferrite reduction with carbon monoxide [J]. Journal of Thermal Analysis and Calorimetry, 2021, 146(5): 2253−2260.
[22] PENG Ning, PAN Qing-lin, JIANG Guo-min, LIANG Yan-jie, WANG Gong-liang, CHEN Yu-jie, MA Guo-ying, MA Tian-chi. Isothermal kinetics of zinc ferrite reduction using a CO−CO_2−Ar gas mixture [J]. Thermochimica Acta, 2020, 686: 178564.
[23] ZHANG Sheng-fu, ZHU Feng., BAI Chen-guang., WEN Liang-ying, PENG Hai-jun. High temperature pyrolysis behaviour and kinetics of lump coal in COREX melter gasifier [J]. Ironmaking & Steelmaking, 2014, 41(3): 219−228.
[24] MOZAMMEL M, SADRNEZHAAD S. K, KHOSHNEVISAN A, YOUZBASHIZADEH H. Kinetics and reaction mechanism of isothermal oxidation of Iranian ilmenite concentrate powder [J]. Journal of Thermal Analysis and Calorimetry, 2013, 112(2): 781−789.
[25] DILMAÇ N. Isothermal and non-isothermal reduction kinetics of iron ore oxygen carrier by CO: Modelistic and model-free approaches [J]. Fuel, 2021, 296: 120707.
[26] LIU Zhong-suo, WANG Qi, ZOU Zong-shu, TAN Guang-lei. Reaction mechanism of carbon gasification in CO_2 under non-isothermal conditions [J]. Journal of Thermal Analysis and Calorimetry, 2011, 104(3): 1091−1096.
[27] OMRAN M, FABRITIUS T, HEIKKINEN E P, VUOLIO T, YU Y W, CHEN G, KACAR Y. Microwave catalyzed carbothermic reduction of zinc oxide and zinc ferrite: Effect of microwave energy on the reaction activation energy [J]. RSC Advances, 2020, 10(40): 23959−23968.
[28] LI Gang, DING Chen-yi, XUAN Sen-wei, LV Xue-wei, WU Shan-shan. Non-isothermal reduction kinetics of calcium ferrite and hematite [J]. Chinese Journal of Engineering, 2018, 40(11): 1317−1324. (in Chinese)
[29] JAYASEKARA A S, MONAGHAN B J, LONGBOTTOM R J. Dispersion of lime in coke analogue and its effect on gasification in CO_2 [J]. Fuel, 2016, 182: 73−79.
[30] LV Wei, GAN Min, FAN Xiao-hui, JI Zhi-yun, CHEN Xu-ling, YAO Jia-wen, JIANG Tao. Recycling utilization of zinc-bearing metallurgical dust by reductive sintering: reaction behavior of zinc oxide [J]. JOM, 2019, 71(9): 3173−3180.
[31] LI Gang, LV Xue-wei, DING Cheng-yi, ZHOU Xuan-geng, ZHONG Da-peng, QIU Gui-bao. Non-isothermal carbothermic reduction kinetics of calcium ferrite and hematite as oxygen carriers for chemical looping gasification applications [J]. Applied Energy, 2020, 262: 114604.
[32] BINNEMANS K, JONES P T, FERNÁNDEZ Á M, TDRRES V M. Hydrometallurgical processes for the recovery of metals from steel industry by-products: A critical review [J]. Journal of Sustainable Metallurgy, 2020, 6(4): 505−540.
[33] YU Ge, YU Dun-xi, LIU Fang-qi, YU Xin, HAN Jing-kun, WU Jian-qun, XU Ming-hou. Different catalytic action of ion-exchanged calcium in steam and CO_2 gasification and its effects on the evolution of char structure and reactivity [J]. Fuel, 2019, 254: 115609.
[34] LAN Chen-chen, LIU Ran, ZHANG Shu-hui, LYU Qing, GAO Yan-jia, YAN Guang-shi. Influence mechanism of CaO on gasification characteristics and kinetic behaviors of carbon-CO_2 reaction [J]. Fuel, 2022, 311: 122583.

CaO 对铁酸锌还原过程中锌迁移机制和动力学的影响

王伟安，邱国兴，王建立，贺 芸，李小明

西安建筑科技大学 冶金工程学院，西安 710055

摘 要：研究 CaO、还原时间和还原温度对 Zn 迁移机制和动力学模型的影响。结果显示，CaO 通过促进中间产物 ZnO 在 Fe 和 CaO 混合物表面的析出和富集，提高锌的挥发率。添加 CaO 后，$ZnFe_2O_4$ 还原步骤为 $ZnFe_2O_4$→$Ca_2Fe_2O_5$→FeO→Fe。$ZnFe_2O_4$ 还原的挥发模型从一阶化学反应模型(不添加 CaO)转变为三维扩散模型(添加 CaO)，表观活化能从 313.9 kJ/mol 降低到 91.77 kJ/mol，为锌的高效还原和挥发提供有利条件。

关键词：含锌粉尘；铁酸锌；还原动力学；迁移机制；直接还原；锌回收

(Edited by Xiang-qun LI)